Cylindrical magnetron discharges. I. Current-voltage characteristics for dc- and rf-driven discharge sources

G. Y. Yeom and John A. Thornton[a)]
University of Illinois, Coordinated Science Laboratory, Urbana, Illinois 61801

Mark J. Kushner[b)]
University of Illinois, Gaseous Electronics Laboratory, 607 East Healey, Champaign, Illinois 61820

(Received 18 July 1988; accepted for publication 5 January 1989)

Direct current magnetron discharge sources are often characterized by current-voltage characteristics of the form $I \propto V^n$ where n is typically in the range from 4 to 10. Similar I-V characteristics are found for dc hollow cathode discharges where the cathode configuration effectively provides electrostatic confinement of the primary electrons. Therefore, by analogy, it has been suggested that the exponent n provides an index to the effectiveness of the magnetic electron confinement in a magnetron discharge. When magnetron discharge sources are driven at rf frequencies, the I-V characteristics typically yield n values in the range 1–3. We have examined the I-V characteristics of cylindrical-post magnetron discharge sources of various diameters driven dc and at rf frequencies of 1.8 and 13.56 MHz. The rf-driven discharges yielded n values which, in most cases, were less than 2.5. Electrostatic probe measurements of the interelectrode voltage distribution showed that the low n values, that is, poor confinement, could be explained by the effect of the magnetic field on the electron transport during that portion of the rf cycle when the post electrode is serving as the anode.

I. INTRODUCTION

Magnetron discharges are low-pressure plasma devices in which an externally applied magnetic field confines electrons, thereby reducing their rate of loss by diffusion. The conductivity of such devices is therefore enhanced over that in the absence of the magnetic field. Typical gas pressures are in the range of 10^{-1}–10^{0} Pa and the degree of ionization is in the range of 10^{-4}–10^{-3}. Direct current magnetron discharge sources are characterized by a current-voltage characteristic of the form $I \propto V^n$, where n is typically in the range from 4 to 10, as shown by curve A in Fig. 1.[1] Similar behavior is seen for elongated nonmagnetron hollow cathode discharges (curve B in Fig. 1). In these devices the anodes are placed at one or both ends of the cathode and electrons are electrostatically trapped within the tubular cathode. Thus, by analogy, it has been suggested that the exponent n in the current expression for magnetron discharges provides an index to the efficiency of electron confinement.[1–3]

When magnetron discharge sources are driven at rf frequencies, the discharge I-V characteristics typically yield n values in the range from 1 to 3,[3–8] lower than that for dc magnetrons. Such values are typical of those found for planar diode discharges driven using either dc (Fig. 1, curve C) or rf power (Fig. 1, curve D). Accordingly it has been concluded that rf-driven magnetron discharges do not operate in the magnetron mode.[3]

This paper reports on a systematic investigation of the current-voltage characteristics for cylindrical-post magnetron discharges[1] having various diameter cathodes that were driven dc, and at rf frequencies of 1.8 and 13.56 MHz. The rf-driven discharges did indeed yield current-voltage characteristics with low n values. Electrostatic probe measurements of the interelectrode voltage distributions were made to investigate this effect. The results suggest that the low n values can be explained, at least for the case of the rf discharges, by the effect of the magnetic field on electron transport to the center cylindrical-post electrode when it serves as an anode. In a companion paper[9] the formation of dc biases in rf magnetrons is discussed to further investigate these issues.

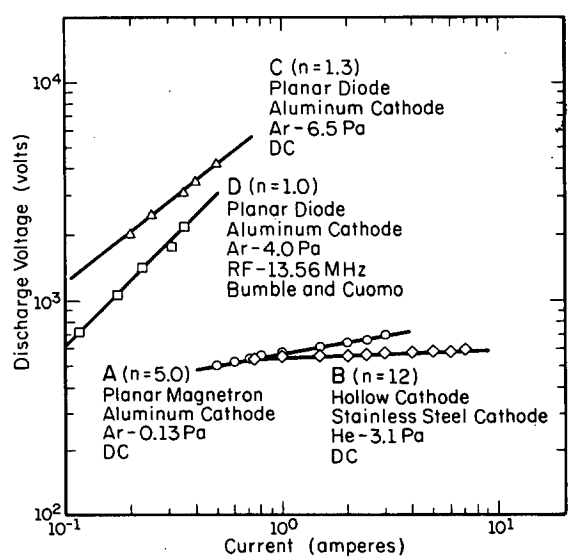

FIG. 1. Current-voltage relationships for various discharge configurations. In all cases the current-voltage relationship has the form $I \propto V^n$, where I is the discharge current and V is the discharge voltage. Data for curves A and C are from Ref. 3. Data for the hollow cathode, curve B, is from Ref. 7. Data for the rf-driven planar diode is from Ref. 8.

[a)] Deceased.
[b)] Author to whom correspondence should be addressed.

 0021-8979/89/103816-09$02.40

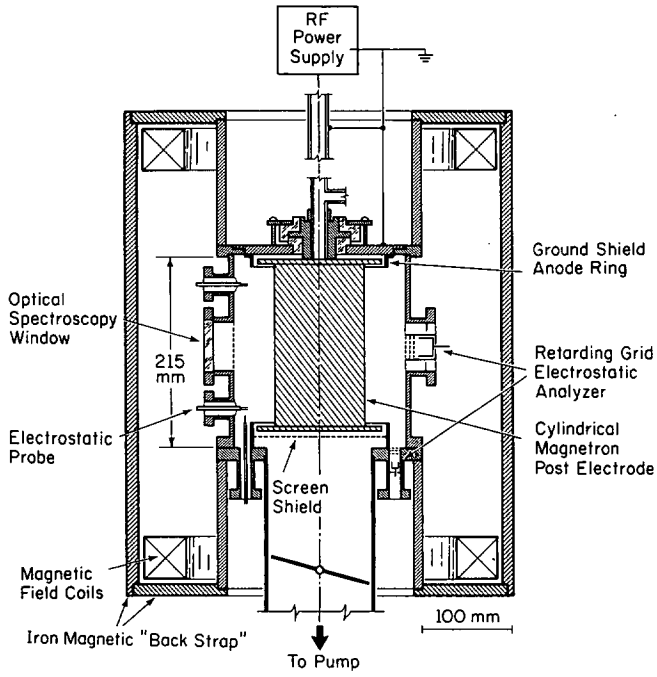

FIG. 2. Schematic drawing of the experimental apparatus.

In Sec. II we will describe the experimental apparatus. We will discuss our results for measurements of I-V characteristics, plasma potential, and plasma density in Sec. III. The implications of these results are discussed in Sec. IV.

II. EXPERIMENTAL CONFIGURATION

The apparatus used for the experiments is shown schematically in Fig. 2. The chamber is constructed of type 304 stainless steel and is configured to accomodate axially mounted flange-type cylindrical-post magnetron electrodes of various diameters. Schematics of the post electrodes that were used for the present study are in Fig. 3. These electrodes were also fabricated from stainless steel. Magnetic field coils are arranged at each end of the chamber in a magnetic backstrap configuration providing field strengths of $\leqslant$250 G. The applied magnetic field was relatively uniform ($\pm$ 10%) and parallel to the electrodes in the region occupied by the post electrode, while leaving the chamber walls accessible to plasma diagnostics instrumentation. Screens were placed over all of the chamber ports so that the grounded discharge chamber provided a relatively well-defined cylindrical hollow electrode.

Current-voltage measurements were made using dc and rf excitation (1.8 and 13.56 MHz), with both Ar and He as working gases. The rf frequencies were selected to perform experiments over a parameter space that included both near resistive (low-frequency) and capacitive (high-frequency) sheath behavior.[10–13] Working gas pressures were varied over the range from 0.13 to 1.3 Pa. Absolute pressures were measured using an MKS (390HA-00001) capacitive manometer. The discharge voltages were measured using a high-impedence probe (Tektronix P6015) having a 75-MHz bandwidth. The discharge currents were measured by a Pearson Electronics Model 411 probe (bandwidth 40 MHz). rms voltages and currents were calculated from oscilloscope traces, and band-filtered signals were used to determine the phase relationship between the voltage and current. The 1.8-MHz power supply was a Henry Electronics Inc. 5KPGA with a T-type matching network. The 13.56-MHz power supply was a Plasma Therm Inc. HFS 10,000D with an L-type matching network. In both cases the post electrodes were capacitively driven through a blocking capacitor and with the chamber grounded. The 1.8-MHz system was tuned by minimizing the plate current at a given power level. The 13.56-MHz system was tuned by minimizing the reflected power.

Ports for electrostatic probes were located in the chamber side walls and base plate as shown in Fig. 2. An additional probe port (not shown) was located on the chamber wall at the cathode midplane. This probe port was used for most of the measurements reported in this paper. Two probe configurations were used. The first was a single probe consisting of a 0.25–0.64-mm-diam $\times$ 5–10-mm-long tungsten electrode mounted in a 6-mm-diam tubular quartz support. The second was a double probe consisting of two 0.5-mm-diam $\times$ 5-mm-long tungsten electrodes mounted in a 6-mm-diam twin-bore ceramic tube having a separation of 3 mm. In both cases protective sleeves were used to shield the insulating surfaces from the sputtered metal atoms.[14] In the dc cases, the single probe was used for measuring the ion density (from the ion saturation current), the electron temperature, the floating potential, and the plasma potential. In the rf cases, the probe was used for measuring the radial distribution in the floating potential and for estimating the ion density and electron temperature. The double probe was used to measure the temporal variations in ion saturation current with rf excitation and therefore provide an estimate of the ion density variations.

A retarding grid electrostatic analyzer located on the chamber wall at the cathode midplane (see Fig. 2) was used to measure the energy distribution of ions incident on the chamber wall as a check of the electrostatic probe plasma potential measurements. The details of the analyzer are shown in Ref. 9.

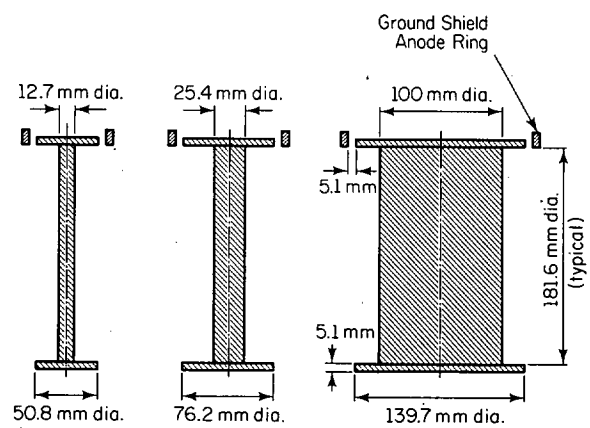

FIG. 3. Schematics of the cylindrical-post "flange-type" magnetron electrodes used in this study.

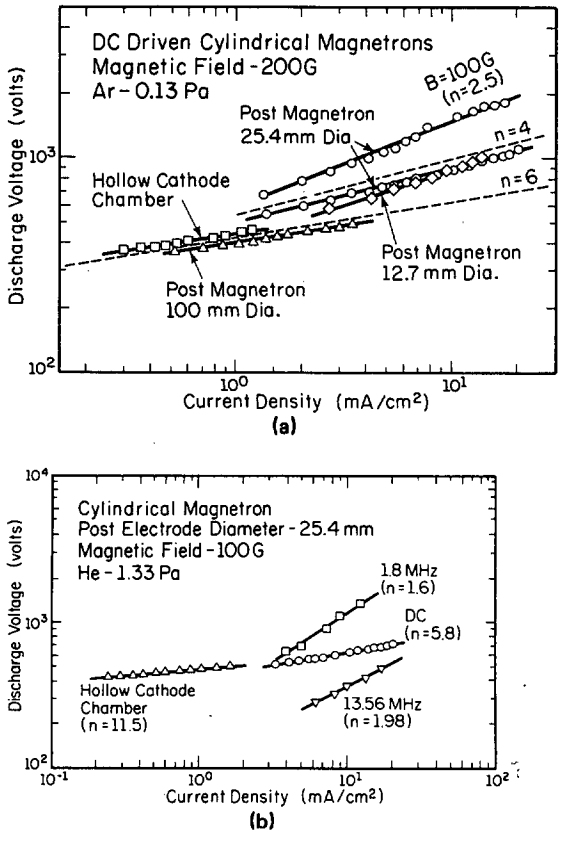

FIG. 4. Current-voltage relationships (as in Fig. 1) for cylindrical magnetron sources shown in Fig. 3 when driven (a) with dc power for Ar and (b) with dc and rf power for He. Also shown in (a) is the effect of magnetic field strength on the current-voltage characteristic for the 25.4-mm-diam electrode.

III. RESULTS

A. Current-voltage characteristics

Direct current-voltage characteristics for the three cylindrical-post magnetrons operated in Ar at 0.13 Pa with an axial magnetic field of 200 G are shown in Fig. 4(a) (bottom curves). Also shown are data obtained when the chamber was driven as a hollow cathode magnetron by biasing the central post electrodes positively as an anode. The data, which are plotted as a function of current density, show that all four magnetrons fall on a nearly common curve of the form $I \propto V^n$ with n in the range from 4 to 6.

The smaller-diameter cylindrical-post magnetrons likely have lower n values because the magnetic field strength was not large enough to satisfy the design condition that the cyclotron radius for the primary electrons, r_c be small compared to the diameter d of the cathode.[1] Thus, for example, r_c/d is about 0.4 for the 12.7-mm-diam electrode compared to about 0.04 for the 100-mm- diam electrode. The top two curves in Fig. 4(a) show the effect of the magnetic field strength in increasing the n value for dc operation of the 25.4-mm-diam magnetron. Thus we expect that an increased magnetic field would have placed all four of the cylindrical magnetrons shown in Fig. 4(a) on a common I-V characteristic with an n value of about 6, which would agree with the results of Ref. 1 (Fig. 14).

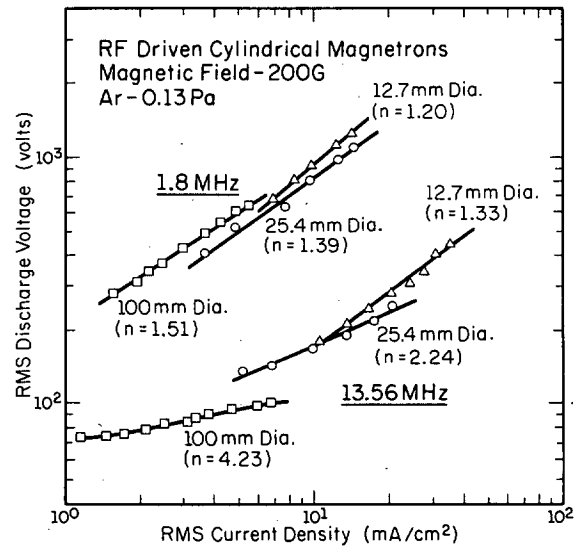

FIG. 5. Current-voltage relationships (as in Fig. 1) for cylindrical magnetron sources shown in Fig. 3 when driven with rf power.

I-V characteristics for operating the discharges as rf cylindrical-post magnetrons with frequencies of 1.8 and 13.56 MHz are shown in Fig. 5. The gas was Ar at 0.13 Pa. The magnetic field strength was 200 G. Typical current, voltage, and floating potential waveforms are shown in Fig. 6. The current typically led the voltage, and the phase difference between the positive peaks of the current and voltage was smaller than that between the negative peaks. Part of the phase differences of these peaks was due to the capacitance of the system which was estimated to be about 30, 40, and 80 pF for the 12.7-, 25.4-, and 100-mm-diam electrodes, respectively. The rms discharge voltages were generally less than 1000 V, and therefore typical of magnetron operation. However with the exception of the magnetron having a large diameter electrode driven at 13.56 MHz, the n values were in the range from 1 to 2.2. The large diameter (100 mm) electrode yielded a magnetron-type I-V curve at 13.56 MHz with an n value of about 4.2.

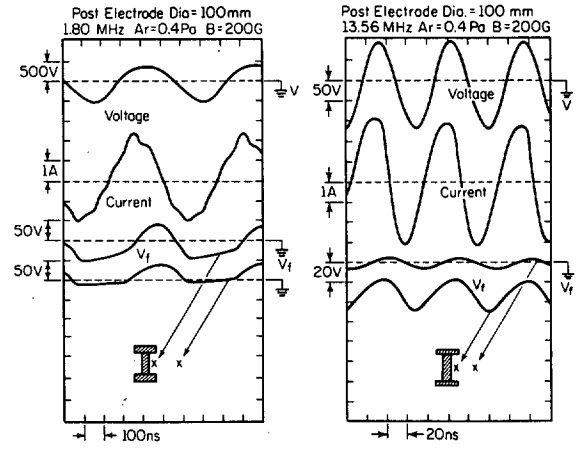

FIG. 6. Discharge voltage, discharge current, and floating potential for the 100-mm-diam electrode driven at 1.8 MHz(left) and 13.56 MHz(right). Schematics of the cathode and end flanges show where the measurements were made. The general trends were independent of the electrode size.

dc and rf current-voltage characteristics for the 25.4-mm-diam magnetron operated in the He at 1.3 Pa are shown in Fig. 4(b). The data again yield consistently high n values for the dc-driven post and hollow cathode cases, but low n values when rf power was used.

B. Plasma potential

To determine the cause of the low n values associated with rf operation, the interelectrode potential distribution was examined for both the dc and rf cases. Starting with the dc case as a point of reference, Figs. 7(a) and 7(b) show the floating and plasma potential as a function of radial position for the 25.4- and 100-mm post-electrodes biased negatively as cathodes or positively as anodes. The working gas was Ar. The plasma potential values were calculated from the electron collection characteristics obtained using the single Langmuir probe. Figure 7(a) (top) shows that the positive anode bias on the 25.4-mm-diam post-electrode did indeed induce a positive space-charge discharge with the chamber serving as a cathode, even though the axial magnetic field was 200 G. The plasma potential (V_p) throughout the chamber was about 300 V above ground. The flanges on the post-electrode (see Fig. 3) provide a rather complex anode geometry in which electrons entering at the circumference can move freely along the axial magnetic field lines to the end flanges. The plasma potential data in Fig. 7(a) (top) suggest that there is indeed a slight gradient in potential (radial electric field) within the region of the end flanges. The floating potential (V_f) was within about 80 V of the plasma potential throughout the major portion of the plasma volume. The electrostatic probe characteristics gave linear log-current versus bias voltage behavior at the onset of electron collection, thereby implying a reasonably well-defined electron temperature (T_e). The indicated value was in the range from 10 eV at points outside the end flanges to 15 eV at points inside the region of the end flanges, which is consistent with the prediction of the relation $V_p - V_f = (kT_e/2e)\ln(M_i/2.3m_e)$,[15] which yields $V_p - V_f \sim 5kT_e$ for Ar. Higher electron temperatures were indicated in the region within the anode flanges and appear to be from electron heating due to the nonradial local electric field.

Figure 7(a) (bottom) shows the plasma and floating potential as a function of radial position with the 25.4-mm post electrode serving as the cathode in a conventional cylindrical magnetron. The plasma potential variation is consisted with the visual observation that the plasma is largely terminated at the anode ring (see Fig. 2). The measured electron temperature was about 3–5 eV within the region of the end flanges and 1–2 eV between the end flanges and the chamber wall.

Figure 7(b) shows similar floating and plasma potential data for the 100-mm-diam post electrode. Floating potential versus radial position data are given for two different magnetic field strengths for the case where the post electrode was operated as a cathode in a conventional cylindrical magnetron (bottom). The measurements of floating potential indicate a potential drop across the magnetically confined plasma that increased with increasing magnetic field strength.

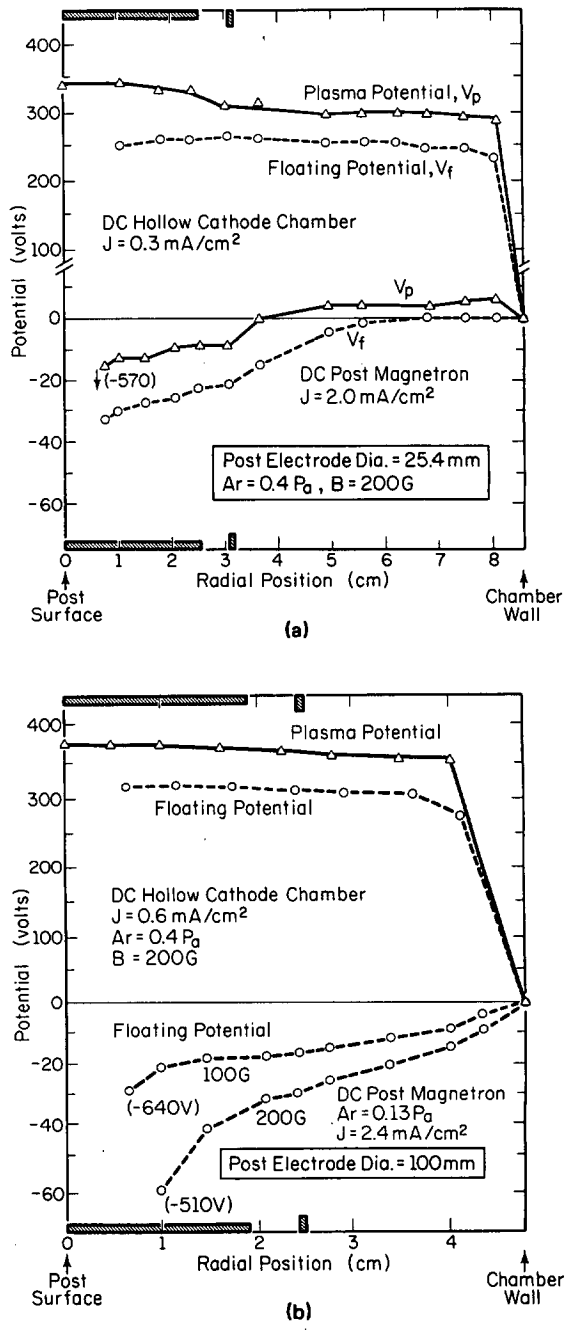

FIG. 7. Plasma and floating potential vs radial position along the vertical midplane for dc discharges (a) with the 25.4-mm-diam post electrode biased as the anode (top curves) and as the cathode (bottom curves) and (b) for the 100-mm-diam electrode with the same biasing. The operating voltages for negatively biased cathode operation are given in parentheses. The hatched regions show the extent of the end flanges on the cathode.

Since the total voltage drop decreased with increasing magnetic field, these results imply that the sheath potential at the cathode decreases at even a higher rate with increasing magnetic field. This observation is consistent with a reduction in electron mobility with increasing magnetic field. The plasma also expands beyond the anode ring as indicated by the floating potential distribution. This is believed to be due to a slight nonuniformity in the magnetic field at large radii and the fact that the annular space between the anode ring and the chamber wall, for the 100-mm-diam electrode, is only about 2.5 cm.

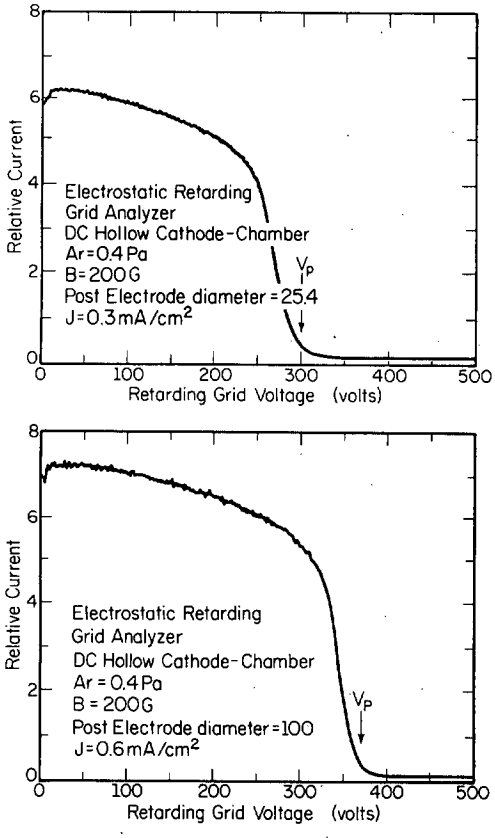

FIG. 8. Retarding grid electrostatic analyzer data for discharges operating under conditions of positive electrode bias as given in Fig. 7.

Although the floating and plasma potential measurements described above were self-consistent, there is always concern over the interpretation of electron collection characteristics when electrostatic probes are operated in magnetic fields of sufficient strength to cause effective electron confinement. Therefore, the probe measurements were supplemented by electrostatic analyzer measurements in which the ion energies incident on the midplane of the grounded chamber wall were measured. The maximum ion energy measured in this manner should be equal to the difference between the plasma potential in the region adjacent to the analyzer and the grounded wall potential. Typical data for hollow cathode operation corresponding to conditions for Fig. 7 are shown in Fig. 8. In both cases the maximum ion energy is in good agreement with the difference between the plasma potential and the grounded cathode potential obtained by probe measurements, 300 V for the 25.4-mm electrode and 370 V for 100-mm electrode. Thus we believe that the plasma potential measurements made with the probe are essentially correct, and that floating potential measurements can be used with a 50–80-V correction for the hollow cathodes and a 10–20-V correction for the post cathodes as an approximation of the plasma potential.

When an rf potential was used to drive the magnetrons, the floating potential was observed to oscillate, essentially in phase with the voltage applied to the post electrode at points within the end flanges. The floating potential appeared somewhat out of phase with the voltage at points outside the end flanges with the applied voltage leading the floating potential. Typical data are shown in Fig. 6. As discussed previously, the floating potential is below the plasma potential by the amount determined by local electron temperature. However, at 1.8 MHz the floating potential should follow the plasma potential, since both ions and electrons can cross the probe sheath in times that are short compared to the oscillating period.[10] The temporal variations in floating potential observed at 1.8 MHz were of the form one would expect for when the sheaths at the electrodes were largely resistive. Similarly, the floating potential variations at 13.56 MHz were suggestive of the sheaths at the electrodes were largely capacitive in nature.[9–12]

The positive and negative extremes of the floating potential as a function of radial position are shown in Fig. 9(a) for the 25.4-mm-diam post electrode driven at frequencies of 1.8 MHz (top curves) and 13.56 MHz (bottom curves). The working gas was Ar at 0.4 Pa and the magnetic field strength was 200 G. Estimates of the electron temperature were made in the 13.56 MHz case from the electrostatic probe measurements. The data indicate that the average electron temperature was in the range from 6 to 10 eV and depended on radial position (generally, the electron temperature was higher closer to the post electrode). Accordingly an average plasma potential, calculated from the mean floating potential and the estimated electron temperature, is also shown in Fig. 9(a).

Similar measurements of the floating sheath potential are shown in Fig. 9(b) for discharges using the 100-mm-diam post cathode operated at 1.8 MHz (top curves) and 13.56 MHz (bottom curves). For 13.56-MHz excitation electron temperatures were measured to be about 6–11 eV and showed a similar dependence on radial position as discharges using the 25.4-mm-diam post electrode. Accordingly, average plasma potentials calculated from the electron temperature and average floating potential are also given in Fig. 9(b). The implication of these results are discussed in Secs. III D and IV.

C. Plasma density measurements

The ion density in the plasma was estimated from measurements of the electrostatic probe ion saturation current, using the theory of Laframboise.[16,17] The ion density was measured instead of the electron density because it is nearly a linear function of the ion saturation current and considerably less sensitive to the electron temperature which is known to vary as a function of position. The measured ion densities were in the range from 2 to 8×10^9 cm^{-3} for low-current density dc hollow cathode discharges having conditions corresponding to Fig. 7. For dc cylindrical-post magnetron discharges (conditions also given in Fig. 7) ion density increased to $(2–8)\times10^{10}$ cm^{-3}. The average ion densities were in the range from 1 to 3×10^{10} cm^{-3} for the rf-driven discharges shown in Figs. 9 when the magnetic field was 200 G. The densities decreased to $1–5\times10^9$ cm^{-3} when the magnetic field was zero.

The dependence of the average ion density on radial position is given in Fig. 10 for a 12.7-mm-diam electrode driven at 13.56 and 1.8 MHz. The position of the maximum in the

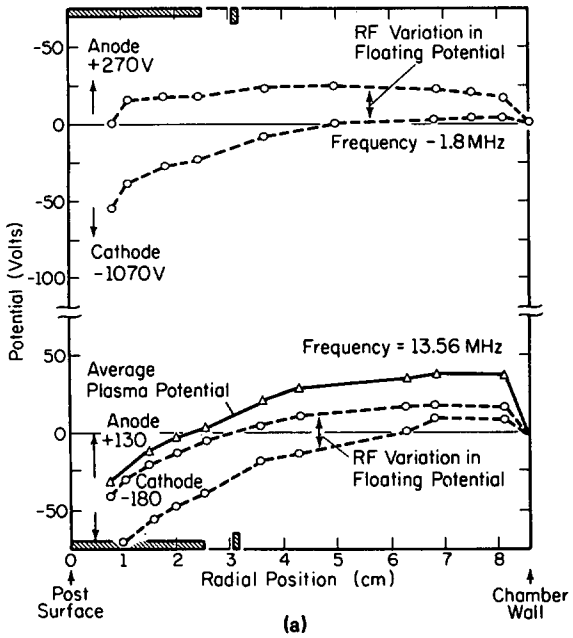

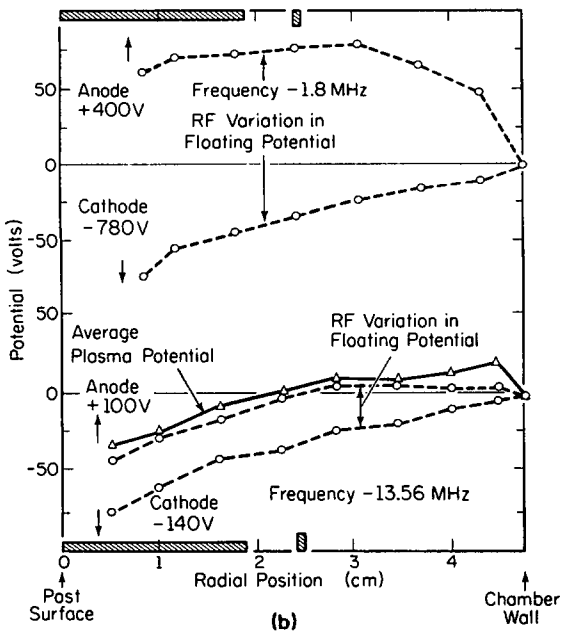

FIG. 9. Maximum positive and negative floating potential excursions vs radial position along the vertical midplane for discharges with (a) the 25.4-mm-diam post electrode and (b) the 100-mm-diam post electrode driven at 1.8 MHz (top curves) and 13.56 MHz (bottom curves). The current density is 3 mA/cm^2, Ar pressure is 0.4 Pa, and the magnetic field is 200 G. The "anode" and "cathode" voltages given on the figure are the peak positive and negative voltage excursions of the post electrode. All voltages are given relative to the grounded chamber. The average plasma potential at 13.56 MHz is calculated from the mean floating potential and the electron temperature. The hatched regions show the extent of the end flanges on the cathode.

ion densities shifted inward towards the post-electrode from the outside of the end flanges when the magnetic field was increased from 0 to 200 G. This movement of the peak position is believed to be partly caused by the decrease in the Larmor radius of the secondary electrons emitted from the

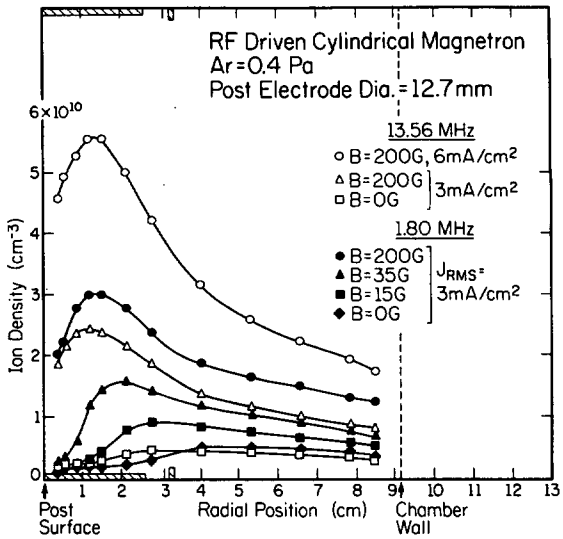

FIG. 10. Dependence of the ion densities on radial position along the vertical midplane for the discharges using a 12.7-mm-diam post electrode driven at 13.56 and at 1.8 MHz. The open circles are for operation at 13.56 MHz, and closed circles are for 1.8 MHz.

post electrode during the cathodic portion of the cycle. In addition, the dc bias of the system and the thickness of the dark space decreased with increasing magnetic field.[9] This indicates that the emitted secondary electrons are less energetic after passing through the sheath and therefore have a shorter range as the magnetic field increases. The region of ionization therefore moves towards the post.

D. Temporal variations in plasma density

The measurements of plasma and floating potential for the rf-driven discharges described above reveal two important features. First, when the post-electrode-voltage swing is negative (i.e., cathode bias), the radial distribution of poten-

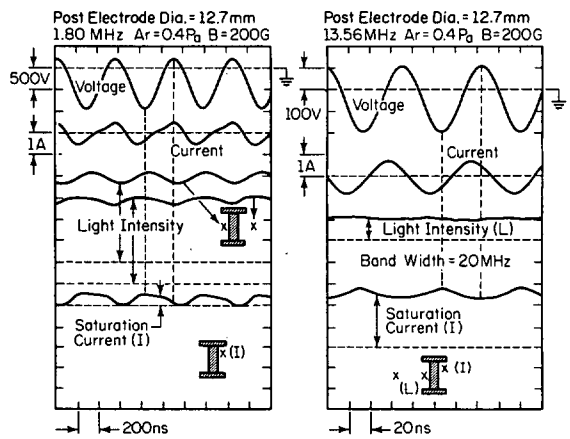

FIG. 11. Discharge voltage, discharge current, light emission from an Ar discharge, and ion saturation current to a double probe. The discharge uses the 12.7-mm-diam electrode operated at 1.8 MHz(left)and 13.56 MHz(right). The signals are band filtered (20 MHz). The hatched schematic shows the cathode with end flanges, and the location of the measurements.

tial is essentially the same as a normal dc-driven cylindrical magnetron discharge. This can be seen by comparing Fig. 9 with Fig. 7 (bottom traces). Second, when the post-electrode-voltage swing is positive (i.e., anode bias), a large voltage gradient developed adjacent to the post electrode with the plasma potential throughout most of the discharge remaining relatively low compared to the post-electrode potential. A double layer appears to form near the post. This was verified by electrostatic analyzer measurements which showed that there were rather large voltage differences between the maximum ion energies incident on the chamber wall and the positive peak potentials of the post electrode under rf excitations.[9] A comparison of the profiles of the maximum positive floating potential for the rf excitation (Fig. 9) with those for dc excitation [Fig. 7 (top traces)] indicates that the discharge does not operate as a hollow cathode chamber on the portion of the rf cycle when the post is positive. The one exception may be for the 100-mm-diam post at 1.8 MHz. In fact, the discharge may not be self-sustained during this portion of the cycle. This behavior was further investigated by observing the time variation of the light emission, and the ion current collected by a negatively biased (-90 V) electrostatic double probe. These measurements were made at points within and outside the end flanges of the 12.7- and 100-mm-diam cylindrical magnetron electrodes during operation at 1.8 and 13.56 MHz.

The light emission measurements were made through the window shown in Fig. 2. A $f/25$ lens system focused light from the plasma onto the photocathode of a Hamamatsu R446 photomultiplier (wavelength sensitivity from 185 to 870 nm). The light intensity is proportional to the rate of electron excitation of the radiative states in Ar, and to their radiative transition probabilities. Typical results for the time dependence of emission are shown in Figs. 11 (12.7-mm-diam electrode) and 12 (100-mm-diam electrode). A weak modulation of about 10% in the light intensity is seen at 1.8 MHz for the 12.7-mm-diam cathode and a weaker modulation of about 5% at 1.8 MHz for the 100-mm-diam electrode. No modulation was detected for either electrode at 13.56 MHz. The fact that the modulation was relatively weak is believed to be due in part to the spontaneous emission life times for many of the prominent Ar emission lines in the visible spectrum which are long compared to the drive frequencies of 1.8 and 13.56 MHz.[18] The important point for the present discussion is that the Ar light intensity with the 12.7-mm-diam electrode at 1.8 MHz was modulated at the discharge frequency and not twice the applied frequency. An increase in light intensity was seen when the voltage swing was negative corresponding to post-magnetron operation, but no increase in intensity was seen when the voltage swing was positive, which corresponds to hollow cathode operation. For the 100-mm-diam electrode driven at 1.8 MHz, a slight modulation corresponding to operation as a hollow cathode discharge was observed when the rf voltage swing was positive. This may be a result of there being a high enough potential (about 300 V) developed near the chamber wall to excite a discharge even though there is a large voltage gradient adjacent to the post electrode.[9]

are shown in Figs. 11 and 12 for the 1.8- and 13.56-MHz

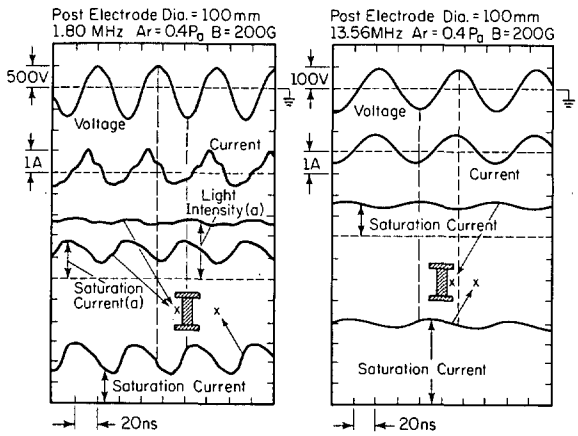

FIG. 12. Discharge voltage, discharge current, light emission from an Ar discharge, and ion saturation current to a double probe. The discharge uses the 100-mm-diam electrode operated at 1.8 MHz(left) and 13.56 MHz(right). The signals are band filtered (20 MHz). The hatched schematic shows the cathode with end flanges and the location of the measurements.

cases. As noted previously, the ion saturation current is nearly proportional to the ion density and relatively weakly dependent on the electron temperature.[16,17] The electron density can be expected to be essentially equal to the ion density because space-charge effects will preclude the monopolar escape of charge species in a continuously operating high-frequency discharge. For the 12.7-mm electrode driven at 1.8 MHz (Fig. 11), the ion saturation current at a point within the electrode end flanges showed a rapid increase as the voltage on the central electrode swung negative to excite post-magnetron operation. The ion saturation current decayed to essentially zero current as the post electrode swung positive as an anode. The probe measurements were similar at points outside the cathode end flanges. Ion saturation currents for the 100-mm-diam electrode are shown in Fig. 12. Again the probe current increased when the electrode was driven negative as a cathode and decreased when it was driven positive as an anode. However, in this case the ion current at 1.8 MHz did not decay to zero during the anode cycle. The modulation of the ion current during the cycle was 65%. The modulation at a point outside the electrode flanges was about 50%. The probe current decayed slower at this location than at a point inside the end flanges when the rf voltage approached the peak of the anode cycle. At 13.56 MHz the probe current did not decay to zero under positive electrode bias, but did exhibit a modulation having the maximum current being nearly in phase with the negative voltage excursions of the central electrode. For the case of the 12.7-mm-diam electrode (Fig. 11) the modulation was about 15% for the probe within or outside of the electrode flanges. For the 100-mm-diam electrode (Fig. 12) the modulation was about 25% inside the electrode flanges and about 10% outside.

IV. DISCUSSION

Glow-discharge magnetrons of the type generally used for sputtering and discussed in this paper are designed according to a dc concept to have specific configurations and

orientations of the cathode, anode, and magnetic field.[3] The objective is to improve the ionizing efficiency and reduce the rate of electron loss in a region adjacent to the cathode surface. This is accomplished by configuring the cathode geometry and magnetic field such that they act in concert to form an electron trap over the cathode surface that has sufficient symmetry to permit closure of the $\mathbf{E}\times\mathbf{B}$ drift currents.[1] The primary electrons, which leave the cathode surface via secondary emission due to ion bombardment and are accelerated in the cathode dark space, exchange energy through collisional processes as they migrate across the magnetic field towards reach the anode. This energy exchange provides the ionization that sustains the discharge. The anode is ideally positioned to intersect magnetic field lines at the periphery of the trap, and thereby to collect the primary electrons that have given up their energy to the working gas in their migration across the magnetic field.[1-3]

Two potential problems can be anticipated when a magnetron of the type described above is driven with an ac potential. First, a magnetic field that is designed to trap electrons in the vicinity of a given electrode for dc cathode operation may shield directed electrons away from this electrode when the ac potential is reversed and the electrode in question must serve as the anode. Similarly, a magnetic field configuration that is designed to allow a free flow of electrons to a given electrode, so that it will perform effectively as an anode during dc operation, will allow electrons to freely escape when the ac cycle is reversed, and this electrode must serve as the cathode. It should be noted in this respect that it is possible to design magnetrons specifically for ac operation.[19] In such a design electron traps are located at each electrode and joined at their periphery by common field lines so that the anode current flow is not totally frustrated. Thus magnetron mode operation with an n value of ~ 4.5 has been achieved at 1.8 MHz in a cylindrical hollow cathode configured according to this principle.[3]

Thus the magnetron concept is designed to improve the effectiveness of the ionization process in cold cathode dc discharges which are sustained primarily by the ionizing action of secondary electrons that are released from the cathode surface by ion bombardment and accelerated in the adjacent sheath electric field. In contrast, at high frequencies, where ions can move only a small distance during an rf cycle and cathode bombarding energies are much reduced, the glow-discharge ionization is sustained to a greater degree by energetic electrons that are heated within the plasma volume by the oscillating electric fields.[20] Two manifestations of this mode of operation are capacitive sheath behavior and relatively low discharge voltages. Although the magnetron concept is not specifically designed to enhance the high-frequency ionization mechanism, the magnetic field can be expected to reduce wall losses and to promote volume electron heating and ionization in desirable regions adjacent to the electrodes. At lower frequencies within the rf range, the ionization process involves significant contributions from secondary electrons emitted at electrode surfaces,[21,22] and the magnetron influence on discharge performance may be expected to be more direct.

The cylindrical magnetrons driven at 1.8 MHz appear to be operating largely in the secondary electron regime. The time dependence of the floating potentials are typical of resistive sheath behavior (Fig. 6). The negative voltage swings are relatively large (Fig. 9) and indicative of a cathode-driven discharge. The spatial dependence of the plasma and floating potentials suggest that the negative swing of the central electrode drives a cylindrical magnetron discharge that is very similar to that formed under dc conditions. This observation is supported by the ion density measurements. The average ion density values of $1-3\times 10^{10}$ cm^{-3} (Fig. 10) that were measured for the 1.8-MHz discharges at 200 G are typical of dc magnetron discharges operating at similar current densities.

The temporal dependencies of the ion saturation current and light emission for the 12.7-mm-diam electrode at 1.8 MHz (Fig. 11) give evidence of nonoptimal excitation. These measurements indicate that when the voltage of the center electrode swings positive, a reversed polarity hollow cathode discharge, with the chamber serving as a hollow cathode and the post electrode as an anode, does not form. Instead a relatively large voltage (100–200 V) develops adjacent to the anode. This voltage is apparently adequate to draw an electron current that is equal to the ion flux during the remainder of the rf cycle and therefore satisfies the capacitive discharge current conservation requirement. It should be noted that there is a power transfer to the plasma during this positive cycle (see Fig. 6). However, the power is transferred primarily to electrons through the electric field developed near the post electrode which immediately deliver it as heat to the anode electrode rather than producing ionization in the plasma. This is the reason for the ion density decaying to zero as shown in Fig. 11. When the cylindrical magnetron was operated at 1.8 MHz with the 100-mm-diam electrode, the ion saturation current did not decay to zero when the rf electrode was at maximum positive potential, as shown in Fig. 12. The decay of the ion current at points near the wall was slower than that inside the end flanges at the peak of the anode cycle. Also, light emission (Fig. 12) showed modulation at twice the frequency of the applied rf voltage. Therefore, for these conditions a reversed polarity hollow cathode discharge appears to form with the chamber serving as a hollow cathode and the post electrode as an anode. A large voltage drop (>100 V) also developed adjacent to the anode as for the case of operation with the 12.7-mm-diam electrode but the voltage drop seems to be not enough to prevent the hollow cathode discharge during the anode cycle.

The large voltage drop that is required to induce the electron current collection is apparently a consequence of the axial magnetic field which reduces the electron mobility in the radial direction by a factor $[1+(\omega_c/\nu)^2]^{-1}$, where ω_c is the electron cyclotron angular frequency and ν is the total electron collision frequency.[2] For a 200-G field, $\omega_c = 3.5\times 10^9$ rad/s. The total electron-atom collision cross section for 10-eV electrons in Ar is about 2×10^{-15} cm^2. Thus the electron-atom collision frequency at a pressure of about 0.4 Pa is about 3×10^7 s^{-1}. Thus $\omega_c/\nu \sim 115$, and the radial electron current transport can be expected to be reduced significantly. It appears that the large anode voltage drop discussed above is responsible for the low n values when

the cylindrical post magnetrons were driven at 1.8 MHz. During the cathode phase of the rf cycle the magnetron behaved similarly as the dc case.

In the 13.56-MHz cases the discharges appear to be operating largely in the volume electron heating regime. The sheath behavior exhibits a capacitive temporal dependence (Fig. 6). The rms voltages are typically a factor of 4 less than in the 1.8-MHz cases. We believe that the 13.56-MHz discharges are best viewed as high-frequency discharges in a complex annular geometry, rather than rf extrapolations of dc magnetron behavior. The temporal dependencies of the electrostatic probe and light emission measurements show that the electron density is pumped during the cathode voltage swing, but remains relatively high throughout the anode cycle. The n values are generally low ($n < 2.2$) except for the case of the 100-mm-diam post electrode ($n = 4.2$). This high n value is believed to be a consequence of a favorable combination of annular geometry and electric field configuration for volume electron heating. It should be noted that the average ion densities measured for the 13.56-MHz discharges at 200 G were in the range from $1\text{–}3\times10^{10}$ cm^{-3} (Fig. 9) and therefore in the range typically found for dc magnetron discharges. Thus, although these discharges are not believed to be maintained primarily by secondary electrons, the performance was enhanced by the magnetic field configuration.

We believe that the general concepts discussed in this paper also apply to other rf magnetron configurations such as planar magnetrons but that caution should be exercised in making detailed extrapolations.

ACKNOWLEDGMENTS

Professor John A. Thornton died unexpectedly in November 1987. He contributed significantly to this work and we will miss his guidance. The authors wish to express their gratitude to Dr. Alan Penfold for his helpful discussions and suggestions. This work was supported by the Joint Services Electronic Projects Agency under Contract No. N00014-84-C-0149.

[1]J. A. Thornton and A. S. Penfold, *Thin Film Processes*, edited by J. L. Vossen and W. Kern (Academic, New York, 1978), p. 75.
[2]J. A. Thornton, J. Vac. Sci. Technol. **15**, 171 (1978).
[3]J. A. Thornton, Thin Solid Films **80**, 1 (1981).
[4]R. K. Waits, *Thin Film Processes*, edited by J. L. Vossen and W. Kern (Academic, New York, 1978), p. 131.
[5]S. Maniv and W. D. Westwood, J. Vac. Sci. Technol. **17**, 743 (1980).
[6]A. R. Nyaiesh and L. Holland, Vacuum **31**, 315 (1981).
[7]J. A. Thornton (unpublished data).
[8]B. Bumble and J. J. Cuomo, J. Vac. Sci. Technol. A **3**, 667 (1985).
[9]G. Y. Yeom, J. A. Thornton, and M. J. Kushner, J. Appl. Phys. **65**, 3825 (1989).
[10]R. H. Bruce, J. Appl. Phys. **52**, 7064 (1981).
[11]M K. Köhler, J. W. Coburn, D. E. Horne, E. Kay, and J. H. Keller, J. Appl. Phys. **57**, 59 (1985).
[12]K. Köhler, D. E. Horne, and J. W. Coburn, J. Appl. Phys. **58**, 3350 (1985).
[13]S. E. Savas, in *Plasma Processing and Synthesis of Materials*, edited by D. Apelian and J. Szekely (Materials Research Society, Pittsburgh, PA, 1987), p. 35.
[14]J. A. Thornton, J. Vac. Sci. Technol. **15**, 188 (1978).
[15]B. Chapman, *Glow Discharge Processes* (Wiley, New York, 1980), p. 70.
[16]J. G. Lamframboise, University of Toronto Institute of Aerospace Studies Report No. 100 (June 1966).
[17]P. M. Chung, L. Talbott, and K. Touryan, *Electrostatic Probes in Stationary and Flowing Plasmas* (Springer, New York, 1975), p. 14.
[18]H. Olsen, J. Quant. Spectrosc. Radiat. Trans. **3**, 59 (1963).
[19]A. S. Penfold and J. A. Thornton, U. S. Patent 4,041,353 (1977).
[20]V. M. Donnelly, D. L. Flamm, and R. H. Bruce, J. Appl. Phys. **58**, 2135 (1985).
[21]M. J. Kushner, J. Appl. Phys. **54**, 4958 (1983).
[22]M J. Kushner, IEEE Trans. Plasma Sci. **PS-14**, 188 (1986).